AIAA JOURNAL
Vol. 30, No. 7, July 1992

Aerothermodynamics of a 1.6-Meter-Diameter Sphere in Hypersonic Rarefied Flow

V. K. Dogra*
Vigyan Research Associates, Inc., Hampton, Virginia 23666
and
R. G. Wilmoth† and J. N. Moss‡
NASA Langley Research Center, Hampton, Virginia 23665

Results of a numerical study using the direct simulation Monte Carlo method are presented for hypersonic rarefied flow about a 1.6-m-diam sphere. The flow conditions considered are those experienced by a typical satellite in orbit or by a space vehicle during entry. The altitude range considered is that from 90 to 200 km, which encompasses the near continuum, transitional, and free-molecular flow regimes. A freestream velocity of 7.5 km/s is assumed in the simulations. The results show that transitional effects are significant at all altitudes below 200 km, but at 200 km the flow about the sphere attains the free-molecular limit. Very little chemical activity is present above 120 km. Both the stagnation point heat transfer and the sphere drag approach their respective free molecule values at 200 km. Results highlight the thermal and chemical nonequilibrium nature of the flowfield. Nonequilibrium effects on the surface heating and body drag are also investigated.

Nomenclature

A = frontal area of sphere, $\pi d^2/4$
C_D = drag coefficient, $2D/\rho_\infty V_\infty^2 A$
C_F = skin-friction coefficient, $2\tau_w/\rho_\infty V_\infty^2$
C_H = heat transfer coefficient, $2q/\rho_\infty V_\infty^3$
C_i = mass fraction of species i, ρ_i/ρ
C_p = pressure coefficient, $2p/\rho_\infty V_\infty^2$
D = drag of sphere
d = diameter of sphere
Kn = Knudsen number, λ/d
Kn_∞ = freestream Knudsen number, λ_∞/d
M = Mach number
$\bar{M}$ = molecular weight of mixture
p = pressure
q = heat flux
R = universal gas constant, 8.3143 J/mol-K
S_∞ = freestream speed ratio, $V_\infty\sqrt{\bar{M}/2RT_\infty}$
T = thermodynamic temperature
T_{ov} = overall kinetic temperature
T_{rt} = rotational kinetic temperature
T_w = surface temperature
T_t = translational kinetic temperature
T_v = vibrational kinetic temperature
u = x component of velocity
V_∞ = freestream velocity
v = y component of velocity
X_i = mole fraction of species i
x = distance from stagnation point measured parallel to freestream
y = distance from symmetry axis measured normal to freestream
θ = circumferential angle measured clockwise from stagnation point
λ_∞ = freestream mean free path
ρ = density
τ = shear stress

Subscripts
i = ith species
w = surface values
∞ = freestream values

Introduction

THE aerothermodynamics of a sphere has been studied in the flow regime between continuum flow and free-molecular flow (transitional flow) using the direct simulation Monte Carlo (DSMC) method. For this study, the focus is on flight conditions (altitudes of 90–200 km and freestream velocity of 7.5 km/s) for which there are neither experimental nor numerical data available. During the 1960s and early 1970s, the drag and heat transfer of spheres were studied both theoretically and experimentally for the transitional flow regime where the experiments were in ground-based facilities. The experiments[1-5] were made for low-energy flow conditions where the total temperature of the gas was often of the order of 300–600 K. The present calculated results are for flight conditions where

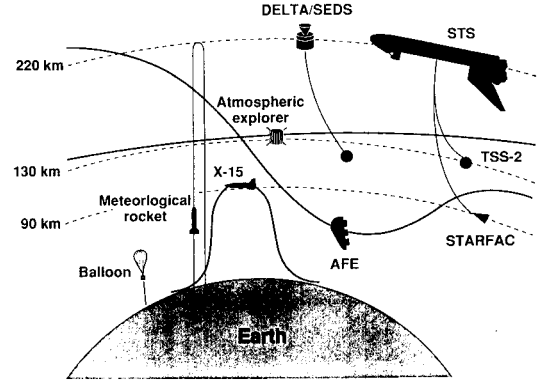

Fig. 1 Altitude access for various measurements platforms.

Presented as Paper 91-0773 at the AIAA 29th Aerospace Sciences Meeting, Reno, NV, Jan. 7-10, 1991; received Feb. 6, 1991; revision received Dec. 17, 1991; accepted for publication Dec. 20, 1991.

*Research Engineer. Member AIAA.
†Research Engineer. Senior Member AIAA.
‡Research Engineer. Fellow AIAA.

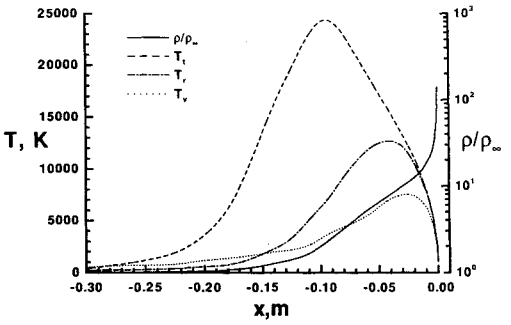

Fig. 2 Flowfield structure along the stagnation streamline (altitude = 90 km, V_∞ = 7.5 km/s, Kn_∞ = 0.01, and T_w = 350 K).

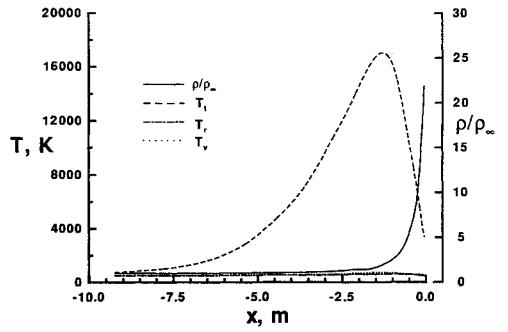

Fig. 3 Flowfield structure along the stagnation streamline (altitude = 130 km, V_∞ = 7.5 km/s, Kn_∞ = 4.83, and T_w = 350 K).

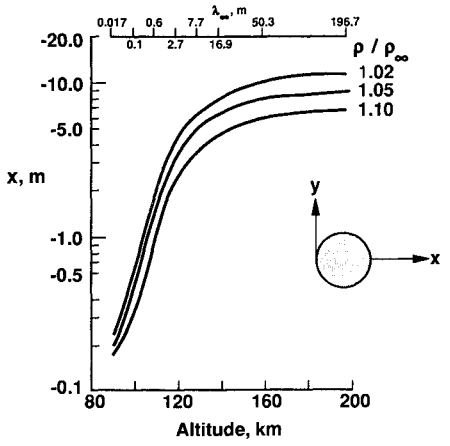

Fig. 4 Location of density increments along the stagnation streamline (V_∞ = 7.5 km/s, d = 1.6 m, and T_w = 350 K).

gas-phase chemical reactions typically become significant for freestream Knudsen numbers less than 0.4.

The motivation of the present study is twofold: first is the continued effort to characterize the translational flow environment for basic shapes (flat plates,[6] blunted[7] and pointed cones,[8] and spheres[9]) for entry flow environments; and second, to provide data to support experiments that potentially will be flown on a tethered satellite system. The Tethered Satellite System-2 (TSS-2) is being proposed as a cooperative effort of NASA and the Agenzie Spaziale Italiana. For this mission, the Shuttle Orbiter would be used to demonstrate a tethered satellite system in a downward deployment and retrieval of a 500-kg, 1.6-m-diam spacecraft attached to the end of a 100-km tether. The tethered spacecraft could reach downward into the outer atmosphere of the Earth to altitudes of 130 km for TSS-2 and later perhaps to 90 km. One of the objectives of the TSS-2 mission is to conduct hypersonic research in the transitional flow regime.

A wide range of engineering studies associated with current and projected space vehicles are concerned with the aerothermodynamics of low-density flows. Flows of particular interest can arise from interactions between two or more of the following events: the vehicle itself, the ambient atmosphere, exhaust plumes from upper stage motors or control motors, and other emitted gas from material outgassing and waste gas venting. Studies concerned with these interactions are receiving added impetus by the Space Shuttle Orbiter flights, the commitment of several nations to pursue the goal of transatmospheric flight with hypersonic slender vehicles, space experiments, technology demonstration programs such as the Aeroassist Flight Experiment (AFE) vehicle and the Tethered Satellite System-2 (TSS-2), the projected space station, and aeroassisted space transfer vehicles (ASTVs).

A common characteristic of the emerging hypersonic transatmospheric vehicles is that they will progress toward maneuverability within the tenuous and largely unknown outer atmosphere in contrast to just passing through it. However, little is known concerning the basic phenomena associated with aerothermodynamics of vehicles in this flight regime. Furthermore, the ground-based facilities are extremely limited in simulating such flow environments because of the need to simultaneously achieve appropriate velocities, model dimensions, and fluid properties.

Experience with research instruments in the altitude range between 90 and 220 km is quite limited because it is too high for balloons or aircraft and too low for persistent orbiting spacecraft. Figure 1 depicts the regions accessible to several vehicles. Tethered systems could provide long-duration access to this altitude range for conducting hypersonic aerothermodynamic research and flight tests. The TSS-2 is a reusable, tethered subsatellite that could initially be extended to an altitude of almost 130 km. A more versatile system would use an expendable tethered deployer and research craft that is "piggybacked" into the unused payload capacity of the second stage of a Delta II launch vehicle [Small Expendable-tether Deployment System (SEDS)].

The present numerical calculations are for a sphere that has the same dimensions as the proposed TSS-2 craft. The following sections describe the method used to simulate the flight environment and results obtained from the numerical simulations.

Computational Approach

The DSMC method[10,11] models the real gas by some thousands of simulated molecules in a computer. The position coordinates, velocity components, and internal state of each molecule are stored and modified with time as the molecules are concurrently followed through representative collisions and boundary interactions in simulated physical space. The time parameter in the simulation may be identified with physical time in the real flow, and all calculations are unsteady. When the boundary conditions are such that the flow is steady, then the solution is the asymptotic limit of unsteady flow. The computation is always started from an initial state that permits an exact specification such as a vacuum or uniform equilibrium flow. Consequently, the method does not require an initial approximation to the flowfield and does not involve any iterative procedures. A computational cell network is required in physical space only, and then only to facilitate the choice of potential collision pairs and the sampling of the macrosopic flow properties. Furthermore, advantage may be taken of flow symmetries to reduce the dimensions of the cell network and the number of position coordinates that need to be stored for each molecule, but the collisions are always treated as three-dimensional phenomena. The boundary conditions are specified in terms of the behavior of the individual molecules rather than the distribution function. All procedures may be specified in such a manner that the computational time is directly proportional to the number of simulated molecules.

Table 1 Freestream conditions

Altitude, km	ρ_∞, kg/m^3	V_∞, km/s	T_∞, K	Mole fraction X_{O_2}	X_{N_2}	X_O	$\bar{M}$, g/mol	λ_∞, m
90	3.43×10^{-6}	7.5	188	0.209	0.788	0.004	28.80	0.016
100	5.64×10^{-7}	7.5	194	0.177	0.784	0.039	28.24	0.100
110	9.64×10^{-8}	7.5	247	0.123	0.770	0.106	27.22	0.599
120	2.27×10^{-8}	7.5	368	0.084	0.733	0.183	26.16	2.681
130	8.22×10^{-9}	7.5	500	0.071	0.691	0.238	25.43	7.724
140	3.86×10^{-9}	7.5	625	0.062	0.652	0.286	24.82	16.875
160	1.32×10^{-9}	7.5	821	0.049	0.581	0.370	23.76	50.330
200	3.29×10^{-10}	7.5	1026	0.032	0.455	0.514	21.97	196.650

Computational Domain and Boundary Conditions

The computational domain used for the present calculations was large enough so that body disturbances do not reach the upstream and side boundaries. The flow at the downstream outflow boundary is supersonic and vacuum conditions are specified. The flowfield was divided into five regions and a very fine grid resolution was used for the cells.

The cell size was of the order of one-third of the local mean free path. Furthermore, at least five subcells per cell were employed in order to capture the velocity gradient accurately within the cell. The time step used in the calculations was less than half of the cell local mean collision time. Steady state was assumed when the number of molecules in each region achieved a fixed value (within $\pm$ 0.2%). The minimum number of simulated molecules in a cell was 20 at steady state. The final results were obtained through a time-averaged solution over a large number of time steps. The sample size of the molecules in each cell was over 200,000.

The molecular collisions were simulated with the variable hard sphere (VHS) molecular model. This model follows the simple hard sphere angular scattering law. Thus, all directions are equally possible for the postcollision velocity in the center-of-mass frame of reference. However, the collision cross section is a function of the relative energy in the collision. The freestream mean free path was evaluated using the VHS collision model with $T_{ref} = 2880$ K, $d_{ref} = 3.083 \times 10^{-10}$ m, and a value of 0.73 for temperature exponent of viscosity coefficient.

Conditions for Calculations

The freestream flight conditions from 90 to 200 km altitude range are given in Table 1. The atmospheric conditions are those given by Jacchia[12] for an exospheric temperature of 1200 K. The surface temperature of the sphere is assumed to be a constant along the surface and equal to 350 K. The gas-surface interaction is assumed to be diffuse with full thermal accommodation. In addition, the surface is assumed to be noncatalytic.

The present DSMC calculations use the same chemical kinetics model given in Ref. 13 (the species of O_2, N_2, O, N, and NO with 34 chemical reactions).

The freestream parameters along with selected results are summarized in Table 2.

Results and Discussion

Although the results cover an altitude range of 90–200 km, special attention has been focused on the 90- and 130-km altitudes. This is because of the interest in providing data for the TSS-2 experiments that will be flown at 130 km and for defining the flow environment at lower altitudes where subsequent tethers may be deployed.

Flowfield Structures

Figures 2 and 3 present the flowfield structure along the stagnation streamline at altitudes of 90 and 130 km, respectively. At 90 km the steeper gradients in density profile (note the change in the x-coordinate scale between the figures) indicate the onset of the formation of a shock wave and shock layer. However, at 130 km the density profile shows that the shock wave is very diffuse.

These figures also show that there is a considerable amount of thermal nonequilibrium in the shock wave and shock-layer regions as indicated by the fact that the rotational and vibrational temperatures are well below the translational temperature. This difference between the translational and internal

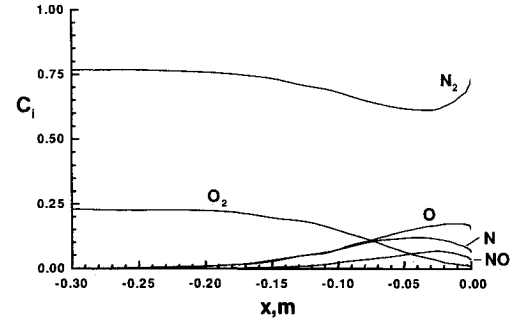

Fig. 5 Chemical composition along the stagnation streamline (altitude = 90 km, $V_\infty = 7.5$ km/s, $Kn_\infty = 0.01$, and $T_w = 350$ K).

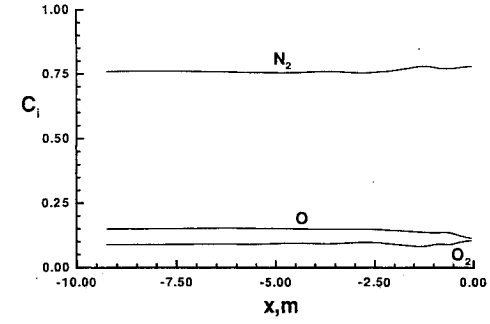

Fig. 6 Chemical composition along the stagnation streamline (altitude = 130 km, $V_\infty = 7.5$ km/s, $Kn_\infty = 4.8$, and $T_w = 350$ K).

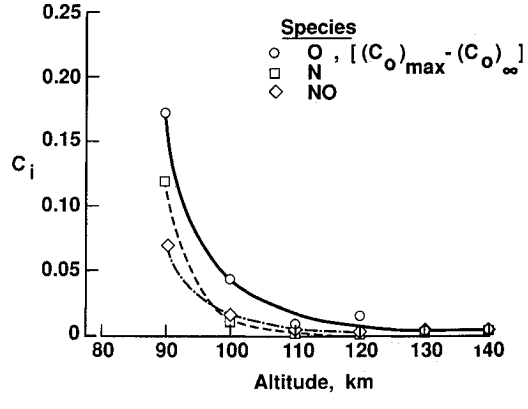

Fig. 7 Maximum species concentration along the stagnation streamline ($V_\infty = 7.5$ km/s, $d = 1.6$ m, and $T_w = 350$ K).

temperatures in the shock layer increases with increasing altitude. At sufficiently high altitudes, the rotational and vibrational modes will remain frozen at the freestream temperature due to the lack of collisions needed to excite the internal modes. Only for the low altitudes and near the stagnation point does the gas achieve thermal equilibrium.

An important consideration in aerothermodynamic analysis is the shock shape and shock standoff distance. Figure 4 shows the location of several density levels (shown as ratios to freestream density) along the stagnation streamline as a function of altitude. It can be seen from these density levels that the disturbance caused by the sphere extends to increasingly large distances upstream with increasing altitude due to the increase in the mean-free path of the molecules. At 200 km, the flow is essentially free molecular and the upstream disturbance ($\rho/\rho_\infty = 1.02$) is of the order of 10 m, whereas at the altitude of 130 km the order is of 7 m. At the lower altitude of 90 km, the upstream disturbance extends to only about 0.25 m.

The chemical composition along the stagnation streamline is presented in Figs. 5 and 6 for five chemical species (O_2, N_2, O, N, and NO) for 90- and 130-km altitude cases. At 90 km, there is a reasonable amount of dissociation upstream of the peak translational temperature with the mass fractions for atomic oxygen and nitrogen achieving values of 0.17 and 0.13, respectively. However, at 130 km there is little chemical activity, and the composition remains essentially constant along the stagnation streamline. The increase in the mass concentration of N_2 near the stagnation point is due to pressure and thermal diffu-

Table 2 Flow parameters and results for a 1.6-m-diam sphere[a]

						Stagnation point	
Altitude, km	Kn_∞	S_∞	Re_∞	M_∞	C_D	C_p	C_H
90	0.010	22.76	3243.00	27.20	1.10	1.91	0.27
100	0.062	22.17	522.30	26.40	1.46	1.97	0.62
110	0.374	19.29	74.80	22.90	1.80	2.08	0.89
120	1.675	15.51	13.20	18.30	1.89	2.14	0.98
130	4.827	13.12	3.80	15.45	1.97	2.15	1.01
140	10.546	11.59	1.52	13.60	2.04	2.15	1.02
160	31.456	9.89	0.43	11.50	2.06	2.14	1.04
200	122.906	8.51	0.10	9.81	2.11	2.16	1.04

[a] $T_w = 350$ K; diffuse surface with full accommodation.

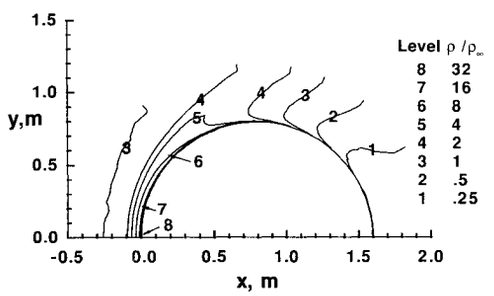

a) Density

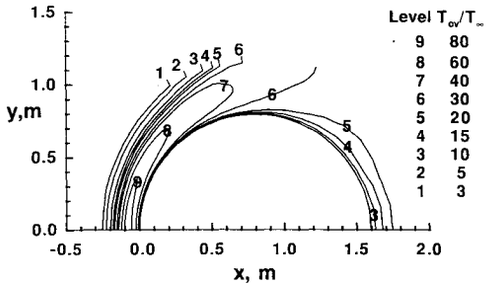

b) Overall temperature

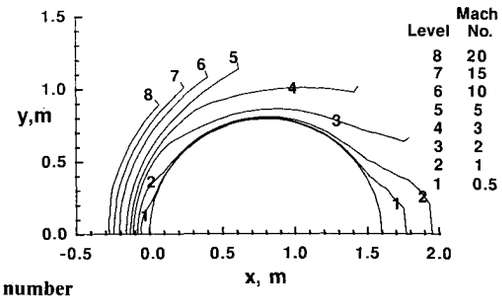

c) Mach number

Fig. 8 Selected contours (altitude = 90 km, $\rho_\infty = 3.43 \times 10^{-6}$ kg/m^3, $T_\infty = 188$ K, and $M_\infty = 27.2$).

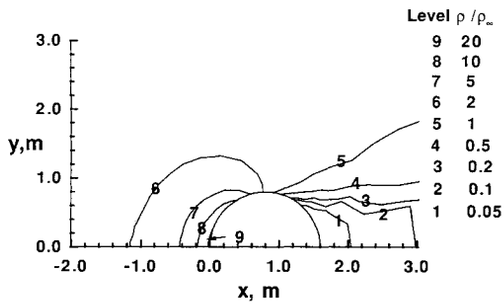

a) Density

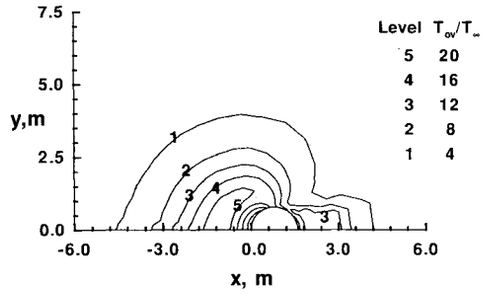

b) Overall temperature

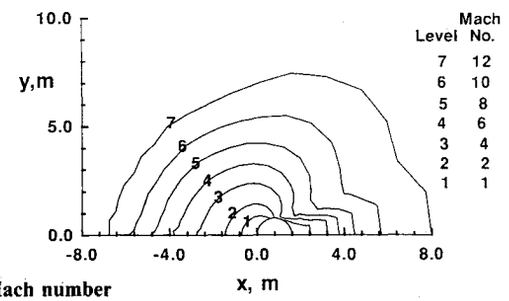

c) Mach number

Fig. 9 Selected contours (altitude = 130 km, $\rho_\infty = 8.22 \times 10^{-9}$ kg/m^3, $T_\infty = 500$ K, and $M_\infty = 15.45$).

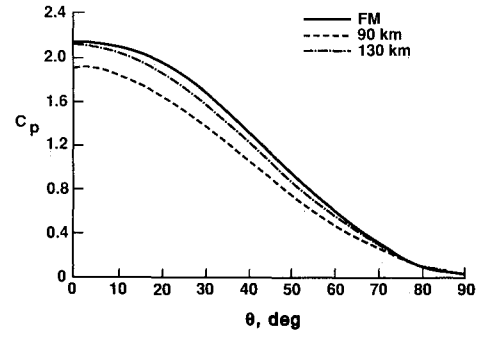

a) Pressure coefficient

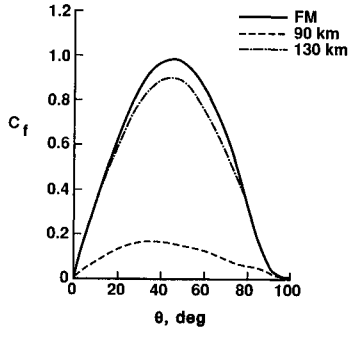

b) Skin-friction coefficient

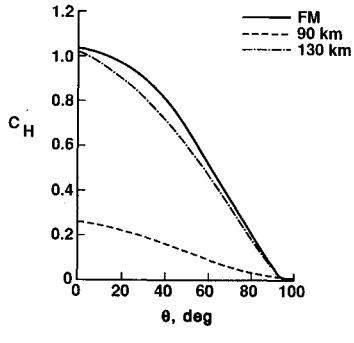

c) Heat transfer coefficient

Fig. 10 Effect of altitude on surface quantities.

sion rather than chemical reactions. As the altitude increases, the level of dissociation decreases until the chemistry is essentially frozen at the freestream composition. This is evident in Fig. 7, which shows the maximum concentration along the stagnation streamline of those species (O, N, and NO) produced primarily by dissociation. It is obvious, from this figure, that very little chemical activity is present above 120 km.

Selected contours of nondimensional density ρ/ρ_∞, the overall nondimensional kinetic temperature T_{ov}/T_∞, and Mach number are shown in Figs. 8 and 9. The density contours for 90-km altitude show (Fig. 8a) that the density rises rapidly near the stagnation point where the density disturbance is confined to a very small region. The density ratio varies from a maximum of about 32 near the stagnation point to values less than 0.25 in the wake. Significant temperature disturbances (Fig. 8b) extend much farther upstream than the density disturbances. The wake is a highly nonequilibrium region, and the high temperatures in the wake are characteristic of a bimodal velocity distribution when two streams of molecules move relative to each other. In this case, slow molecules from the surface are combining with faster molecules coming from the outer region. At 130-km altitude (Figs. 9a and 9b), the density and temperature contours show a more gradual rise of density and temperature as the flow approaches the sphere further showing the diffuse nature of the shock wave that is characteristic of the highly rarefied flow. Also, the density and temperature disturbances for 130-km altitude extend much farther upstream as compared with the 90-km altitude.

Surface Quantities

The surface pressure, skin friction, and heat transfer coefficients are presented in Figs. 10a–10c, respectively, for the forebody of the sphere. The results are plotted as a function of the circumferential angle θ measured clockwise from the stagnation point. The rarefaction effects can be seen by comparing the results for different altitudes shown in these figures with those predicted for the free-molecular (FM) limit. The variation of the pressure coefficient with altitude is moderate for the diffuse gas-surface interactions assumed in the present calculations. In contrast, the skin friction and heat transfer coefficients are very sensitive to rarefaction effects as shown in Figs. 10b and 10c. It is also evident that the flowfield of 130 km cannot be considered completely free molecular. However, at 200 km, the pressure, skin friction, and heat transfer coefficients are the same as the free-molecular values and the flow can be classified as free molecular.

The stagnation-point heat transfer coefficient is presented in Fig. 11 as a function of freestream Knudsen number (and altitude). The results show the expected variation in the transition flow regime; that is, the heat transfer coefficient increases substantially with increasing rarefaction and approaches the free-molecular limit at 200 km. It should be noted, however,

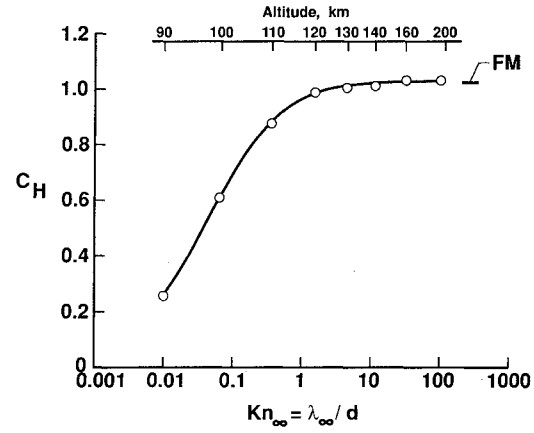

Fig. 11 Effect of rarefaction on stagnation-point heat transfer (V_∞ = 7.5 km/s, d = 1.6 m, and T_w = 350 K).

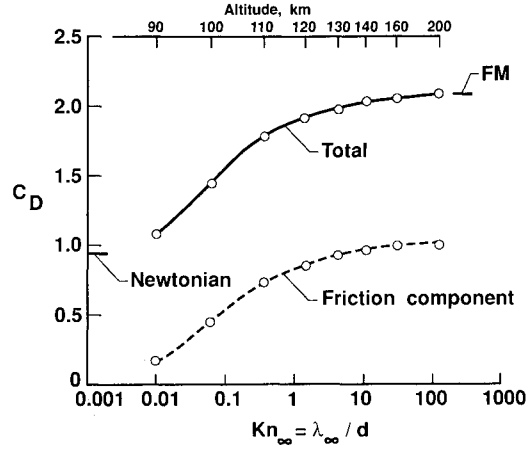

Fig. 12 Effect of rarefaction on drag coefficient (V_∞ = 7.5 km/s, d = 1.6 m, and T_w = 350 K).

that the dimensional heat transfer actually increases with decreasing altitude due to the rise in density.

Sphere Drag

Figure 12 presents calculated total-drag and friction-drag coefficients for the 1.6-m-diam sphere as a function of freestream Knudsen number (and altitude). The total drag coefficient approaches the free-molecular value at 200 km and appears to closely approach the Newtonian value at 90 km. At the higher Knudsen numbers, the friction component of the drag is almost 50% of the total drag but becomes a much lower percentage as the flow approaches the continuum regime at lower Knudsen numbers.

Concluding Remarks

Results obtained with the DSMC method for a 1.6-m-diam sphere show that the flowfield is typically rarefied and that transitional effects persist over the range of conditions considered. Very little chemical activity is present above about 120-km altitude; however, there is considerable dissociation of molecular oxygen at an altitude of 90 km. The internal energy modes are frozen at and above 130 km and at lower altitudes there is considerable nonequilibrium between translational and internal energy modes. At 200 km, the flow about the sphere is essentially free molecular.

The results also have implications with regard to potential measurements of atmospheric and aerothermodynamic properties under the flight conditions studied. First, because of the upstream extent of the density and temperature disturbances caused by the sphere, it would be necessary to closely match the measurement instruments to specific altitudes and to use an analysis method such as DSMC to assist with the extraction of the undisturbed freestream properties. An unobtrusive measurement technique would perhaps be preferred since physical probes tend to introduce an additional disturbance that must be considered. Second, the assumption of diffuse scattering with full thermal accommodation used in the DSMC analysis needs to be verified against experiment at the actual flight conditions. Therefore, measurements that can independently give information on the gas-surface interactions would be needed. Finally, the lack of chemical activity above 120 km suggests that detailed profiles of the gas composition would be needed only at altitudes below this value. Furthermore, DSMC analysis should be an integral part of any detailed experiment design for both atmospheric and aerothermodynamic measurements in the transitional flight regime.

References

[1]Koppenwaller, G., and Legge, H., "Drag of Bodies in Rarefied Hypersonic Flow," *Thermophysical Aspects of Re-Entry Flows,* edited by J. N. Moss and C. D. Scott, Vol. 103, Progress in Astronautics and Aeronautics, AIAA, New York, 1986, pp. 44–59.

[2]Kinslow, M., and Potter, J. L., "The Drag of Spheres in Rarefied Hypervelocity Flow," Arnold Engineering Development Center, AEDC-TDR-62-205, Arnold AFS, TN, Dec. 1962.

[3]Bailey, A. B., "Sphere Drag Measurements in an Aeroballistics Range at High Velocities and Low Reynolds Numbers," Arnold Engineering Development Center, AEDC-TR-66-59, Arnold AFS, TN, May 1966.

[4]Geiger, R. E., "Some Sphere Drag Measurements in Low Density Shock Tunnel Flow," General Electric Co. Space Sciences Lab., Rept. R64 SD23, Philadelphia, PA, July 1963.

[5]Potter, J. L., and Miller, J. T., "Sphere Drag and Dynamics Simulation in Near-Free-Molecular Flow ," *Rarefied Gas Dynamics,* Sixth Symposium, Vol. 1, Academic, New York, 1969, p. 723.

[6]Dogra, V. K., and Moss, J. N., "Hypersonic Rarefied Flow About Plates at Incidence," *AIAA Journal,* Vol. 29, No. 8, 1991, pp. 1250–1258.

[7]Moss, J. N., Cuda, V., and Simmonds, A. L., "Nonequilibrium Effect for Hypersonic Transitional Flows," AIAA Paper 87-0404, Jan. 1987.

[8]Taylor, J. C., Moss, J. N., and Hassan, H. A., "A Study of Hypersonic Flow Past Sharp Cones," AIAA Paper 89-1713, June 1989.

[9]Wood, G. M., Wilmoth, R. G., Carlomagno, G. M., and Luca, L., "Proposed Aerothermodynamic Experiment in Transition Flow Using the NASA/ASI Tethered Satellite System-2," AIAA Paper 90-0536, Jan. 1990.

[10]Bird, G. A., "Monte Carlo Simulation in an Engineering Context," *Rarefied Gas Dynamics,* Pt. I, edited by Sam S. Fisher, Vol. 74, Progress in Astronautics and Aeronautics, AIAA, New York, 1981, pp. 235–239.

[11]Bird, G. A., *Molecular Gas Dynamics,* Clarendon Press, Oxford, 1976, Chap. 7.

[12]Jacchia, L. C., "Thermospheric Temperature Density and Composition: New Models," *Research in Space Science,* Smithsonian Inst. Astrophysical Observatory Special Rept. No. 375, Cambridge, MA, March 1977.

[13]Moss, J. N., and Bird, G. A., "Direct Simulation of Transitional Flow for Hypersonic Re-Entry Conditions," *Thermal Design of Aeroassisted Orbital Transfer Vehicles,* edited by H. F. Nelson, Vol. 96, Progress in Astronautics and Aeronautics, AIAA, New York, 1985, pp. 113–139.